

The Discharge and Corrosion Behavior of Al Anodes with Different Purity in Alkaline Solution

G. S. Peng*, J. Huang, Y. C. Gu, G. S. Song*

Key Laboratory of Green Manufacturing and Surface Technology of Advanced Metal Materials, Ministry of Education, School of Materials Science and Engineering, Anhui University of Technology, Ma'anshan, 243002, P. R. China.

*E-mail: pengguosheng@126.com (G.S.Peng), Song_ahut@163.com (G.S.Song)

Received: 28 March 2020 / Accepted: 7 May 2020 / Published: 10 June 2020

The replacement of high purity Al anodes with low purity Al meanwhile maintaining low self-corrosion and high electrochemical activity is of significance for commercial application of Al-air battery. In this paper, the discharge and corrosion behavior of Al anodes with different purity in alkaline solution were systematically studied by self-corrosion test, electrochemical methods and discharge test. The results show that the self-corrosion resistance is determined by Fe-bearing impurity particles. The electrochemical activity depends on both Fe-bearing impurity particles and the solid solubility of Fe impurity element in Al matrix. Fe-bearing impurity particles play a positive role in activating the oxide film on Al anode. The dissolution of Fe impurity element into solution increases the value of OCP and thereby decreases the operating voltage. Based on the operating voltage and discharged efficiency at the low / high constant current density, 99.99% purity Al anode (4N Al) is considered to be a good choice to prepare Al anode for Al-air battery.

Keywords: Al anode; Self-corrosion; OCP; Polarization curve; EIS; Discharge behavior

1. INTRODUCTION

One of the most promising applications for Al is found to be Al-air batteries, which have special interest for further use in electric vehicles and large-scale energy storage systems [1-2]. The major advantage of this technology compared to other batteries is the fact that Al exhibits a high theoretical voltage (-2.7 V) and a high theoretical energy density of 8076 Wh·kg⁻¹. The low coulombic efficiency of Al anode in strong alkaline media, however, limits its practical implementation. One of problems results from its high self-corrosion. High purity Al as raw materials [3] was developed to decrease the self-corrosion of Al anodes. It inevitably increases the cost for Al-air batteries. Some studies [4-17] focused on the replacement of high purity Al anodes with low purity Al meanwhile maintaining low

2.2 Characterization

The microscopic examinations of Al anodes were performed by scanning electron microscopy (SEM, JEOL-6510LV) and the composition was analyzed using energy dispersive spectroscopy (EDS). The corrosion morphologies were captured via digital camera. The value of electrical conductivity was determined via FQR7501A digital micrometer. The average value of electrical conductivity was obtained by measuring at least five areas of sample.

2.3 Hydrogen evolution tests

Hydrogen evolution tests of Al anodes were conducted in 4 M NaOH solutions at room temperature. An inverted burette with a funnel was used to collect and measure the volume of hydrogen. Al anode samples were cut into slab with a dimension of 10×10×5 mm. The samples were immersed into 4 M NaOH solutions for 30 minutes and the volume of hydrogen was recorded every 2 minutes. The average hydrogen evolution rate of the sample was then calculated according to the following formula (1), where v_{H_2} represents the average hydrogen evolution rate ($\text{mL}\cdot\text{cm}^{-2}\cdot\text{min}^{-1}$), V_{H_2} represents the total volume of hydrogen evolution (mL), S is the surface area of the sample (cm^2), and t is the immersion time (s).

$$v_{H_2} = \frac{V_{H_2}}{St} \quad (1)$$

2.4 Weight loss tests

The treated samples with a dimension of 10×10×5 mm were immersed into 4 M NaOH solutions for 5h. The temperature for the experiments was maintained at 25°C by means of water bath. The weight of the samples before and after immersion was measured after cleaning the corrosion products. The corrosion products of Al anodes were clean-out in solutions of 2% CrO_3 and 5% H_3PO_4 at 80°C for about 5 minutes and then rinsed by distilled water and ethanol. The corrosion rate was calculated using the formula (2) [7, 23], where W is the weight loss, mg; D is the density, g/cm^3 ; A is the surface area, cm^2 ; and T is the time, h. The average value of corrosion rate is obtained by measuring at least three samples.

$$\text{Corrosion rate (mm/yr)} = \frac{87.6W}{DAT} \quad (2)$$

2.5 Electrochemical tests

Electrochemical tests were conducted in a traditional three-electrode cell utilizing Zennium E electrochemical workstation at room temperature. The working electrode is Al anodes with an exposed area of 1 cm^2 . The counter electrode is a platinum foil electrode (10×10 mm), the reference electrode is Hg/HgO (1 M OH⁻), and a Luggin probe was also used. The electrolyte is 4 M NaOH solutions. The polarization curves of the samples were measured after open circuit potential (OCP) was performed for 900 seconds. The potential range was ± 1 V relative to OCP with a scanning rate of 5 mV / s. IR correction

was also performed. For electrochemical impedance spectra (EIS) measurements, a sinusoidal potential of 5 mV amplitude and a frequency sweep of 100 kHz – 0.01 Hz was used as disturbance signal at OCP. The equivalent circuits simulating the electrochemical response of the system were constructed using ZView2 software.

2.6 Discharge behavior tests

The batteries consist of anodes, cathodes and electrolytes. Anodes were made of Al anodes. Cathodes were air electrodes, which were commercial procurement. It contains a double-layer structure of gas diffusion and catalytic layers (MnO_2), laminated with a nickel mesh current collector. The unit was shown in Fig. 1, which is made of PPE (Poly-Phenylene Ether). Each area of anode and cathode exposed to the electrolyte was 4.52 cm^2 under air condition. The electrolyte was 4 M NaOH solutions, which volume was 5 mL. The discharge curve of the Al-air batteries was studied by the constant current discharge of 10 mA / cm^2 and 100 mA / cm^2 for 1 h at room temperature. The Neware test system was used. The weight of the anodes was measured both before and after discharge. The cleaning procedure for corrosion products after discharge is the same as the weight-loss tests did. The anode utilization (η), capacity density and energy density were calculated using the following formulas (3, 4, 5), respectively. [23]:

$$\eta = \frac{100It}{(\Delta m F / 9)}; \quad (3)$$

$$\text{Capacity density} = \frac{Ih}{\Delta m}; \quad (4)$$

$$\text{Energy density} = \frac{UIh}{\Delta m} \quad (5)$$

where η is the anode utilization, %; I is the current, A; Δm is the weight loss, g; F is the Faraday constant; and t is the time, s; U is the average voltage, V; h is the time, h.

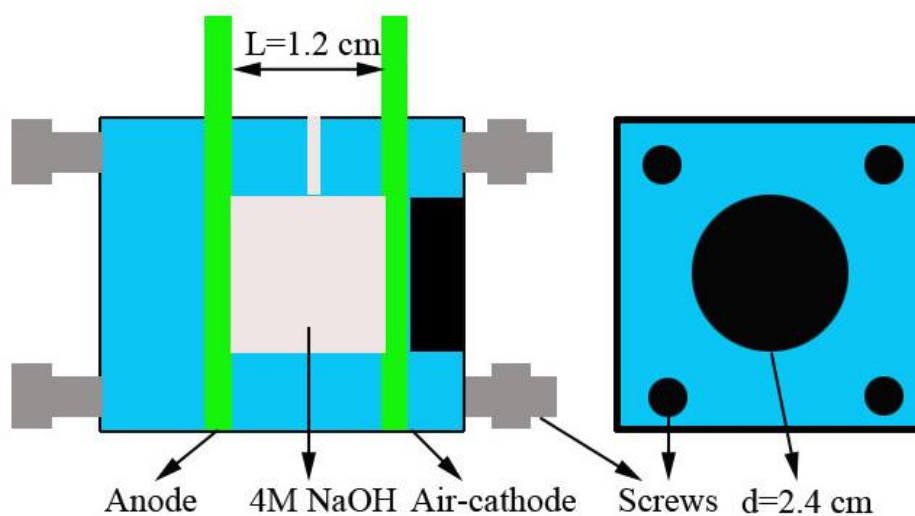


Figure 1. Schematic diagram of full-cell for discharge behavior tests

3. RESULTS AND DISCUSSION

3.1 Self-corrosion behavior

Self-corrosion behavior of three grades purity Al anodes was characterized by hydrogen evolution and weight-loss tests. Fig.2 showed the hydrogen evolution of Al anodes as a function of time in 4 M NaOH solutions. It is clear that, for all anodes, the hydrogen evolution volume lineally increases and then slightly faster increases in the later stage. The hydrogen evolution rate is $0.172 \text{ ml}\cdot\text{cm}^{-2}\cdot\text{s}^{-1}$ for 2N Al, $0.097 \text{ ml}\cdot\text{cm}^{-2}\cdot\text{s}^{-1}$ for 4N Al and $0.073 \text{ ml}\cdot\text{cm}^{-2}\cdot\text{s}^{-1}$ for 5N Al. The hydrogen evolution rate, therefore, is in the order as following: $5\text{N Al} < 4\text{N Al} < 2\text{N Al}$. Fig.3 exhibited the results of weight-loss tests of Al anodes. Obviously, the sequence of weight-loss for three grades purity Al anodes is consistent with the results obtained from hydrogen evolution tests. That is, the self-corrosion rate from weight-loss tests decreases with the increase of purity of Al anodes. Fig.4 showed the typical microstructure of three grades purity Al anodes by SEM morphology observation and EDX analysis. The significant difference among three grades purity Al anodes is the amounts of bright particles. The bright particles in amount increase with the decrease of Al purity. EDX analysis indicates that the composition of bright particles mainly consists of Fe element and little Si element. Since slight Si element has little effect on localized corrosion [26] and the cathodic reaction of Al alloys [27], its roles will be no longer discussed in the subsequent parts. Fe-bearing impurity particles has low hydrogen over-potential [28] and can provide sites for hydrogen evolution. As a result, the hydrogen evolution amount increases as the decrease of Al impurity. Furthermore, Fe-bearing impurity particles are cathodic compared to Al matrix [29], the potential difference between Fe-bearing impurity particles and Al matrix, therefore, leads to the localized corrosion. More Fe-bearing impurity particles result in more dissolution of Al matrix. That is the reason why the corrosion rate from the weight-loss tests increases with the decrease of Al purity.

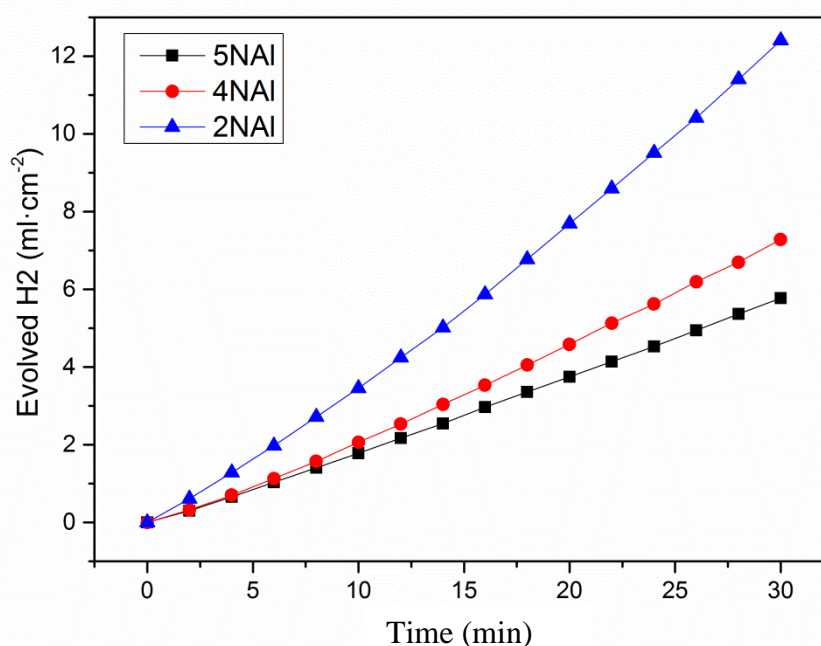


Figure 2. Hydrogen evolution of three grades purity Al anodes as a function of time in 4 M NaOH solutions

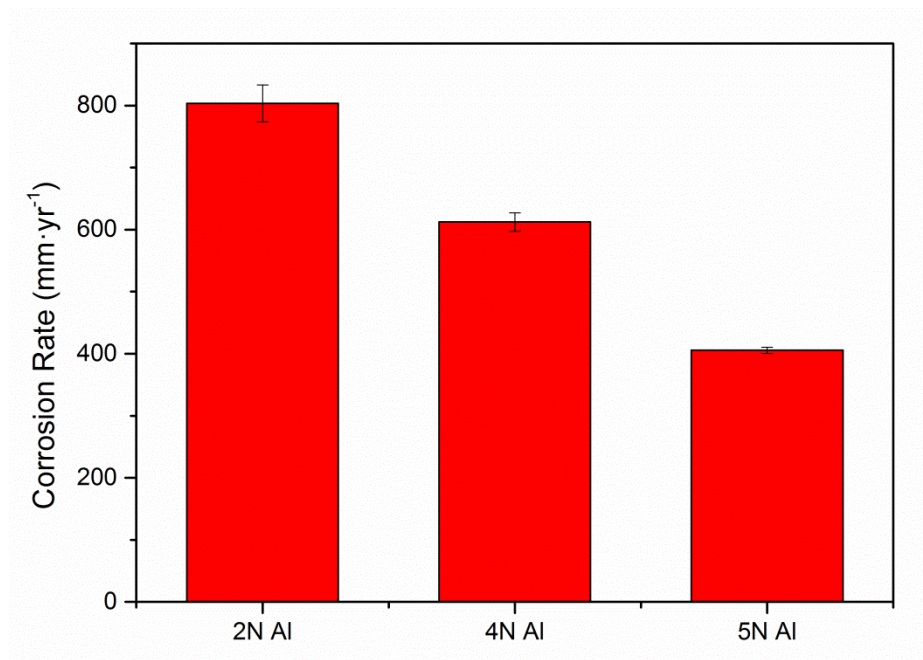


Figure 3. Weight loss results of three grades purity Al anodes after immersing 5 h in 4 M NaOH solutions

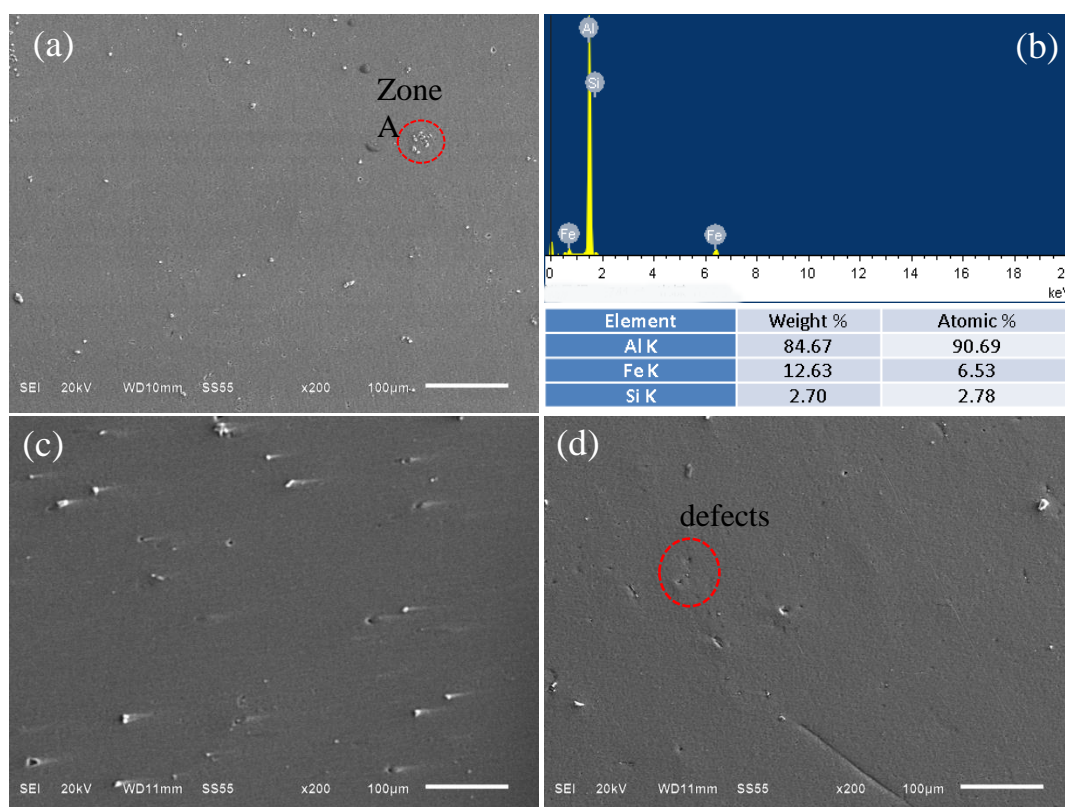


Figure 4. The typical microstructure and EDS analysis for three grades purity Al anodes (a) 2N Al; (b) EDS analysis from Zone A; (c) 4N Al; (d) 5N Al

3.2 Electrochemical behavior

Electrochemical behavior of three grades purity Al anodes was characterized by OCP, polarization curves and EIS. The OCP versus time plots for Al anodes in 4 M NaOH solutions were shown in Fig.5. For all Al anodes, the OCP initially changes to more positive values and then stable. Compared with 2N and 4N Al anodes, 5N Al anode exhibits OCP variation in a wider range, indicating that 5N Al anode has better corrosion resistance in NaOH solutions. This may contribute to less Fe-bearing impurity particles. It is documented that the value of OCP is determined by the solid solution, rather than un-dissolved impurity particles [30]. Since the main impurity element is Fe element, the OCP is determined by the solid solubility of Fe impurity element in Al matrix. A simple way of determining the solubility of impurity element is by electrical conductivity, since impurity element in solid solution depresses the conductivity of Al to a much greater extent than when out of solution [31]. The electrical conductivity is 37 MS/m for 2N Al, 38 MS/m for 4N Al and 39 MS/m for 5N Al, indicating that the solid solubility of Fe impurity element increases with the decrease of Al purity. The variation for electrical conductivity with Al purity can be understood when considering the maximum solubility of Fe element in pure aluminum is about 0.048 wt.% [32]. Compared with Al element ($\text{Al}/\text{Al}^{3+} = -1.66$ vs NHE), the standard electrode potential of Fe element is more positive ($\text{Fe}/\text{Fe}^{3+} = -0.44$ vs NHE) [30]. Therefore, it results in an increase of the mixing potential of Al anodes with the increase of the solid solubility of Fe element. This, in turn, leads to an increase of OCP. Fig.6 exhibited the polarization curves for three grades purity Al anodes. The corrosion parameters from the polarization curves were obtained by the Tafel extrapolation method, as listed in Table 2. It can be seen that the corrosion potential and corrosion current decrease with the increase of Al purity. It can be explained by the Evans diagram, in which the values of corrosion potential and corrosion current from polarization curves are determined by the Tafel anodic and cathodic polarization [33]. For three grades purity Al anodes, the anodic polarization is similar whereas the cathodic polarization is different, as seen in Fig.6. The difference in cathodic polarization contributes to Fe-bearing impurity particles, which play a key role in depolarization of cathodic polarization. Compared to high purity Al anode, the low purity Al anode has lower cathodic polarization, resulting in the higher corrosion potential and corrosion current density. For three grades purity Al anodes, the slope for anodic polarization is steeper than that for the cathodic polarization, indicating that the polarization process is predominated by the anodic polarization (Table 2). The result is consistent with the views by other authors [14]. It indicates that the decrease of anodic polarization is a key step for the activation of pure Al anode, which depends on the properties of oxide film on Al anodes. Fig.7 showed the impedance spectra presented in Nyquist plots for Al anode in NaOH solutions at OCP. The Nyquist diagram displays a complex feature - a high frequency capacitive arc, a middle frequency inductive arc and a low frequency capacitive arc, as shown in Fig.7 (a). According to the views by Brett [34], the high frequency arc must be associated with the electron transfer resistance (R_t) in parallel with the double-layer capacitance (C_d) between the interfaces of metal / oxide. The medium frequency inductive arc is more likely to be the weakening of the protective oxide layer by the adsorbed intermediate (maybe AlOH_{ad}) [35]. The low frequency capacitive arc is related to the reactions in the interface of oxide/electrolyte, producing corrosion product. Hence, the circuit model of this system was shown in Fig.8. It can be seen that there is good compatibility between the experimental and simulated

data by using the model in Fig.7, where dashed line represents experimental data and solid line represents the fitting data. The simulated parameter values were displayed in Table 3. Compared to 4N and 5N Al anode, the R_t of 2N Al is lower. It indicates the electron transfer of 2N Al anode readily occurs and thereby, the electrochemical activity of 2N Al anode is relatively higher. It may attribute to the activation effect of Fe-bearing impurity particles on Al anode, which is in agree with the results by polarized curve. The decrease of C_t with the Al purity can be explained by the definition of capacitance, which is expressed by the following equation:

$$c = \frac{\epsilon_0 \epsilon S}{d} \quad (6)$$

where ϵ_0 is the permittivity of vacuum, ϵ is the relative permittivity of the film, S is the area of surface or interface, and d is the thickness of the film or the double-layer. The decrease of C_t with the increase of Al purity may be due to the increase in the thickness of oxide film on the premise of the same surface area according to equation (6). The increase in the thickness of oxide film may result from the lack of Fe-bearing impurity particles, which thin the oxide film on Al anode. In the case of the C_{lf} and R_{lf} from the low frequency arc, the values are approximately equal, suggesting that the Al purity has little effect on the interface reaction between oxide and electrolyte.

Table 2. Corrosion parameters of different grades of purity Al anodes in 4 M NaOH solution

Materials	E_{corr} (V vs Hg/HgO)	$-\beta_c$ (mV/dec)	β_a (mV/dec)	j_{corr} (mA/cm ²)
2N Al	-1.38	367	528	23.8
4N Al	-1.39	407	564	21.6
5N Al	-1.45	412	598	9.94

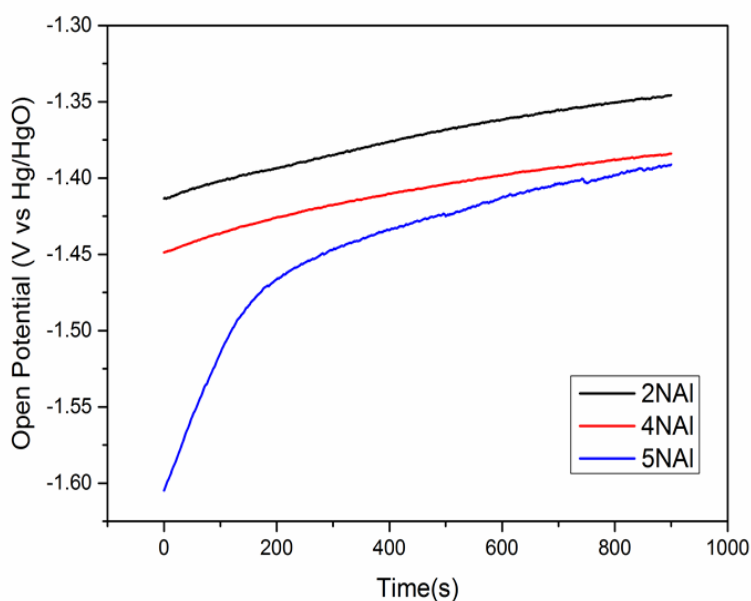


Figure 5. The OCP variation of different grades purity Al anodes in 4 M NaOH solutions

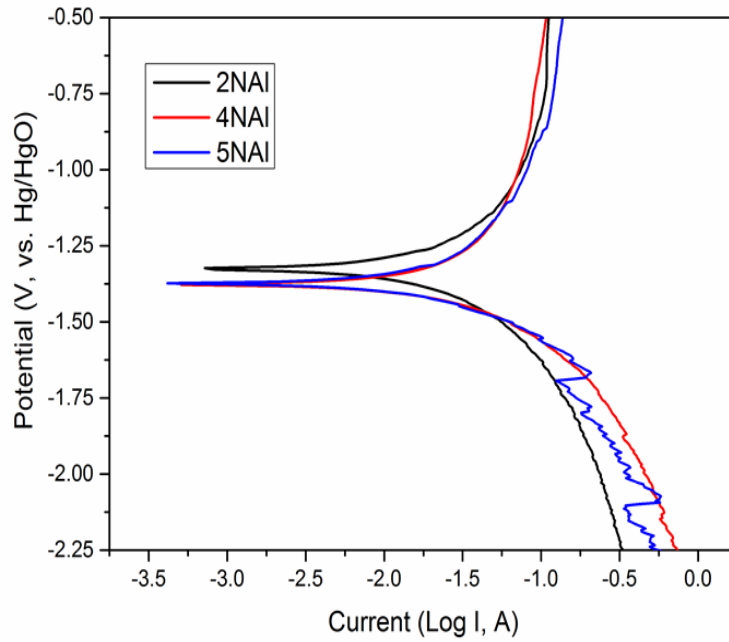


Figure 6. Polarization curves of different grades purity Al anodes in 4M NaOH solutions (a) polarization curve; (b) Evans diagram

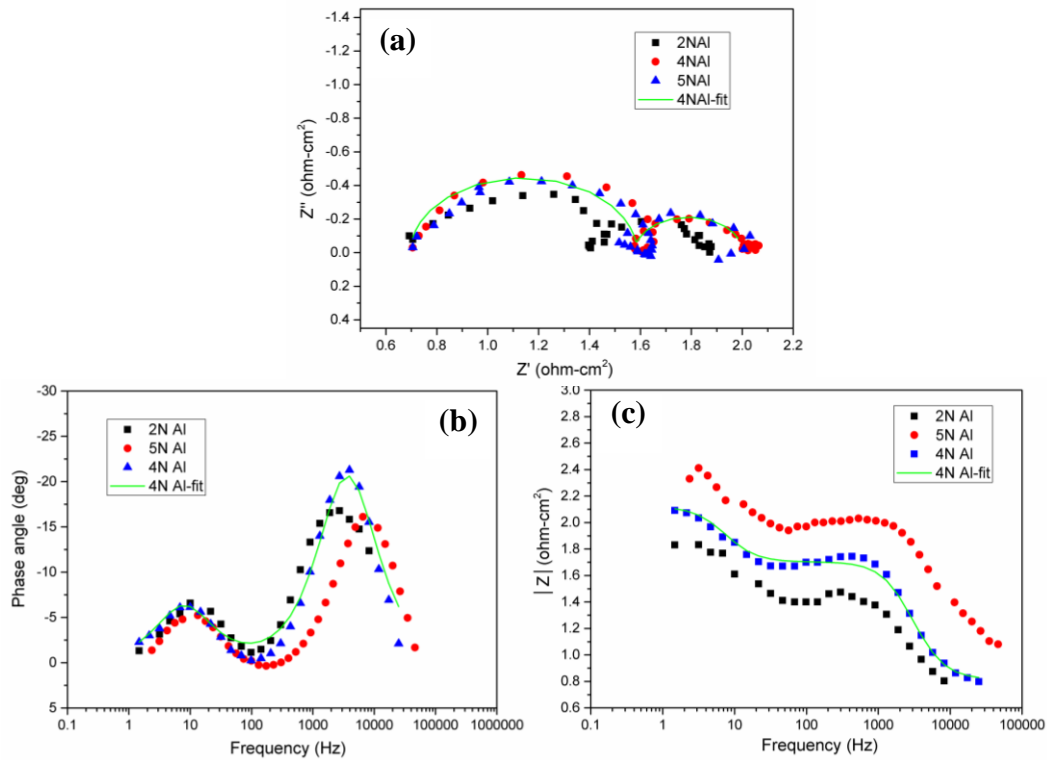


Figure 7. Impedance spectra presented in Nyquist plots of different grades purity Al in 4MNaOH solutions at OCP (a) Nyquist diagram; (b,c) Bode diagram

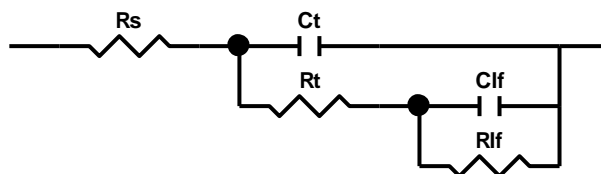


Figure 8. Equivalent electrical circuit for purity Al in 4M NaOH solutions at OCP

Table 3. Simulated EIS information for different grades of purity Al in NaOH solution at OCP

	C_t [$\Omega^{-1}\text{cm}^{-2}\text{S}^{-n}$]	R_t [Ωcm^2]	C_{lf} [$\Omega^{-1}\text{cm}^{-2}\text{S}^{-n}$]	R_{lf} [Ωcm^2]
2N Al	11.391×10^{-5}	0.6849	0.04314	0.3873
4N Al	7.018×10^{-5}	0.9015	0.0477	0.3879
5N Al	3.257×10^{-5}	0.8949	0.0499	0.3867

3.3 Discharge behavior

The discharge behavior of Al anodes was studied by discharging at low constant current density (10 mA / cm²) and high constant current density (100 mA / cm²). Fig.9 showed the discharge curves of Al-air battery at low constant current density, the discharge parameters being shown in Table 4. For all Al anodes, the voltage-time curves are similar. The operating voltage initially decreases and then stabilizes to an approximate constant value. The initial decrease of operating voltage may attribute to the polarization effect by discharge current. The operating voltage of 4N Al anode is highest among three grades purity Al anodes, being 1.18 V. Since OCP represents the potential of Al anode in the static state, the more negative its value is, the higher the electrochemical activity is, thereby the higher the operating potential is [36]. As discussed in section 3.2, the dissolution of Fe impurity element into Al matrix increases the value of OCP. With the increase of Al purity, less Fe impurity element is dissolved into Al matrix, as has been characterized by the electrical conductivity, and thereby the operating potential increases. On the other hand, Fe-bearing impurity particles have a positive effect on the activation of oxide film on Al anodes by accelerating the electron transfer, as has been also verified by EIS in Fig.7. With the increase of Al purity, less Fe-bearing impurity particles are formed. It leads to a decrease of operating potential value. Based on the two counteracting effects of Fe impurity element on the operating voltage, 4N Al anode with the medium Fe content, therefore, has the highest operating voltage. In addition, the discharge efficiency (the anode utilization, capacity density and energy density) is similar for three grades purity Al anodes. The anode utilization of three grades purity anodes is similar with that of Al-0.5Mg [37] and Al-0.075Ca [11] while the capacity density of three grades purity anodes is higher than that of Al-0.5Mg at the same discharge current density [37]. Compared with Al-0.5Mg-0.1Sn-0.02Ga-0.1Si [38], the anode utilization of three grades purity anodes is higher although the operating potential is lower. The variation in the discharge efficiency for three grades purity Al anodes can be explained by the counteracting effect of Fe-bearing impurity particles. The Fe-bearing impurity particles

not only activate the oxide film but also degrade the corrosion resistance. Both factors made three grades pure Al anodes possess similar discharge efficiency at the low constant current density.

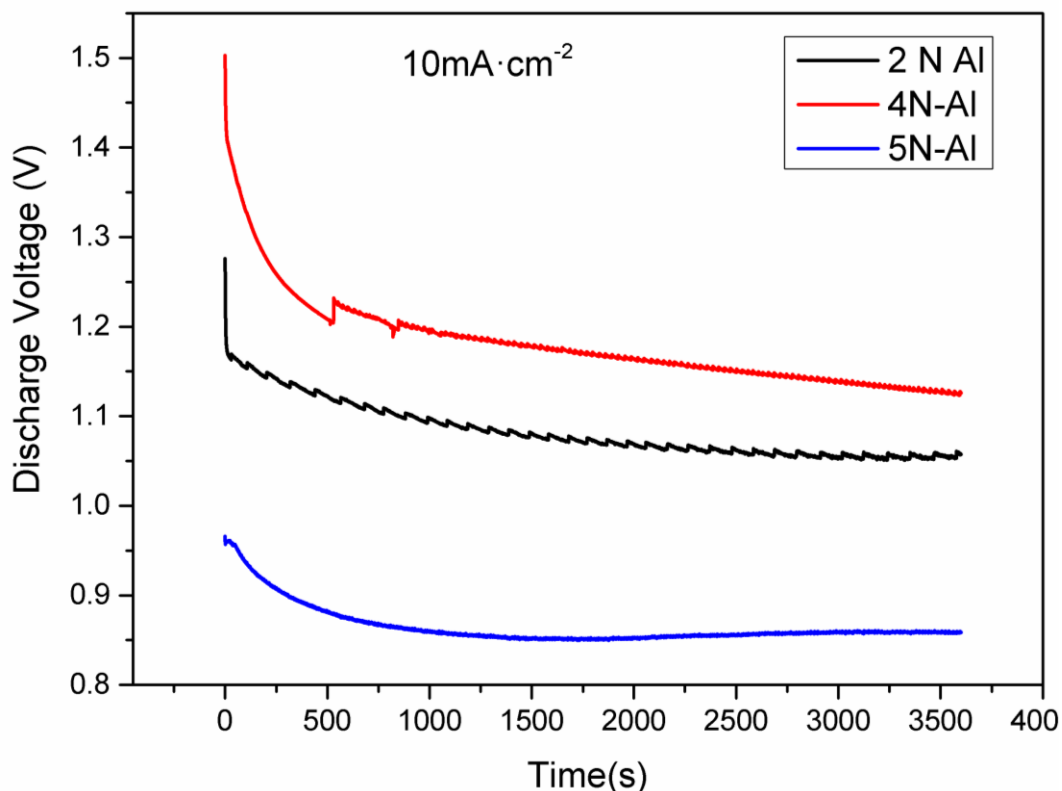


Figure 9. Cell voltage vs time curves of three grades purity Al at current density of $10 \text{ mA}\cdot\text{cm}^{-2}$ for the full-cell in 4 M NaOH solutions

Table 4. Batteries performance parameters for three grades of purity Al discharged at current density of $10 \text{ mA}\cdot\text{cm}^{-2}$

	Average Discharge Voltage(V)	Anode Utilization (η ,%)	Capacity Density ($\text{mAh}\cdot\text{g}^{-1}$)	Energy Density ($\text{Wh}\cdot\text{kg}^{-1}$)
2N Al	1.08	9.9	296	320
4N Al	1.18	8.4	252	298
5N Al	0.86	8.1	241	207

Fig.10 exhibited the discharge morphologies of Al anode. It can be seen that, for three grades purity Al anodes, a generalized corrosion occurs but there are significant differences in localized corrosion underneath the corrosion products. 2N Al anode exhibits more localized corrosion, some obvious cracks being seen. In contrast, 5N Al anode has little localized corrosion replaced by stable passive film, contributing to the synergetic effect of discharged current and few Fe-bearing impurity particles.

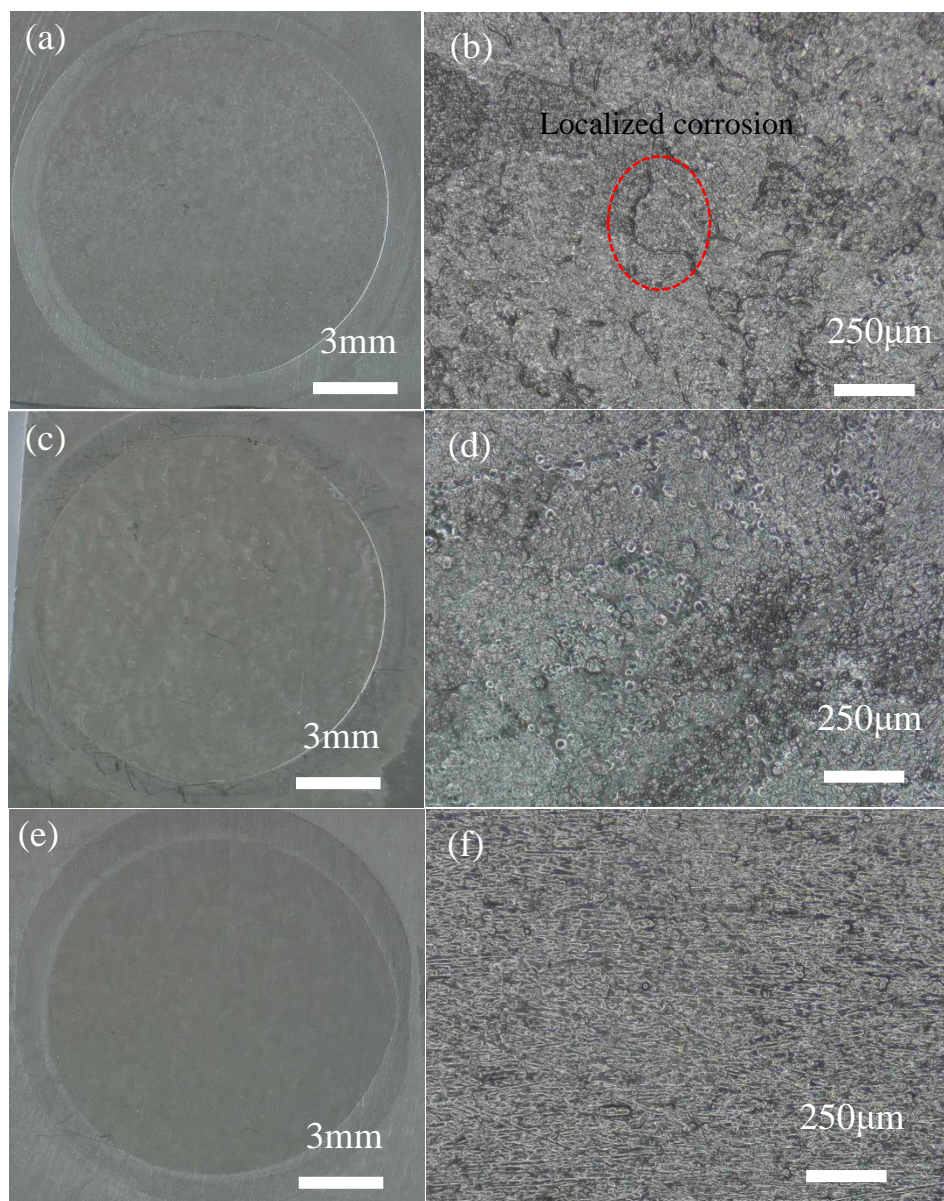


Figure 10. The morphologies of Al anode after discharge at current density of $10 \text{ mA}\cdot\text{cm}^{-2}$ for the full-cell in 4 M NaOH solutions (a,b) 2N Al; (c,d) 4 N Al; (e,f) 5N Al

Fig.11 showed the discharge curves of three grades purity Al anodes at high constant current density. Table 4 summarized the discharge parameters. Compared with discharge at low constant current density, the discharge curve at high current density exhibits more fluctuate and the operating voltage significantly decreases for three grades purity Al anodes. It indicates the anodic polarization of Al anodes become more serious with the increase discharge current density, even no discharge voltage for 5N Al anode. The variation in the operating potential of different grades purity Al anode as a function of discharge current was also studied by Kim et al. [23]. They found that low grade pure Al anode (2N Al) is higher battery efficiency than high grade pure Al anode (5N Al) with decreasing discharge voltage to 0.8 V. They contributed this to high discharge current induced by low discharge voltage accelerate the removal of Fe complex layer. In this studies, 2N Al and 4N Al anode being higher discharge efficiency than 5N Al anode may be explained by the mechanism above when they discharged at high discharge

current. Since the microstructure of 5N Al anode exhibits few Fe-bearing impurity particles underneath initial oxide film, more acute anodic polarization occurs by the high discharge current density relative to other grades purity Al anodes. As a result, there is no operating potential for 5 N Al anode. It should be noted that the discharge efficiency of 2N Al and 4N Al anode at high current density are much higher than those at low current density. It results from the effect of high discharge current. Furthermore, 4N Al anode has better discharge efficiency than 2N Al anode. The anode efficiency of 4N Al anode is 61%, being two times higher than that of 2N Al anode and approaches that of Al-2.7Mg-0.19Cr-0.04Mn at the similar discharge condition [6]. This may be possibly attributed to less weight loss and less hydrogen evolution at high constant current density for 4N Al anode. During the process of discharge, Fe impurity of Al anode are firstly dissolved and Fe ions are formed in the solutions. Subsequently the Fe ions react with Al (or electrons) and formed the Fe complex layer. The Fe complex layer accelerates the hydrogen evolution. Since 2N Al anode contains more Fe impurity element, more Fe complex layer are formed on Al anode. it leads to more hydrogen gases to be released and thereby a decrease in the discharge efficiency. The mechanism above has been found in other Al anode [39,40].

The discharge morphologies well reflect the discharge process (Fig.13). Compared with discharge at low constant current, the passive phenomena for three grades purity Al anodes become more serious when applying high discharged current. It results from the anodic polarization by a high discharge current and leads to a sharp decrease in discharge voltage. The most noticeable case is 5N Al anode, where the whole surface is covered by passive films and no localized corrosion sites can be seen.

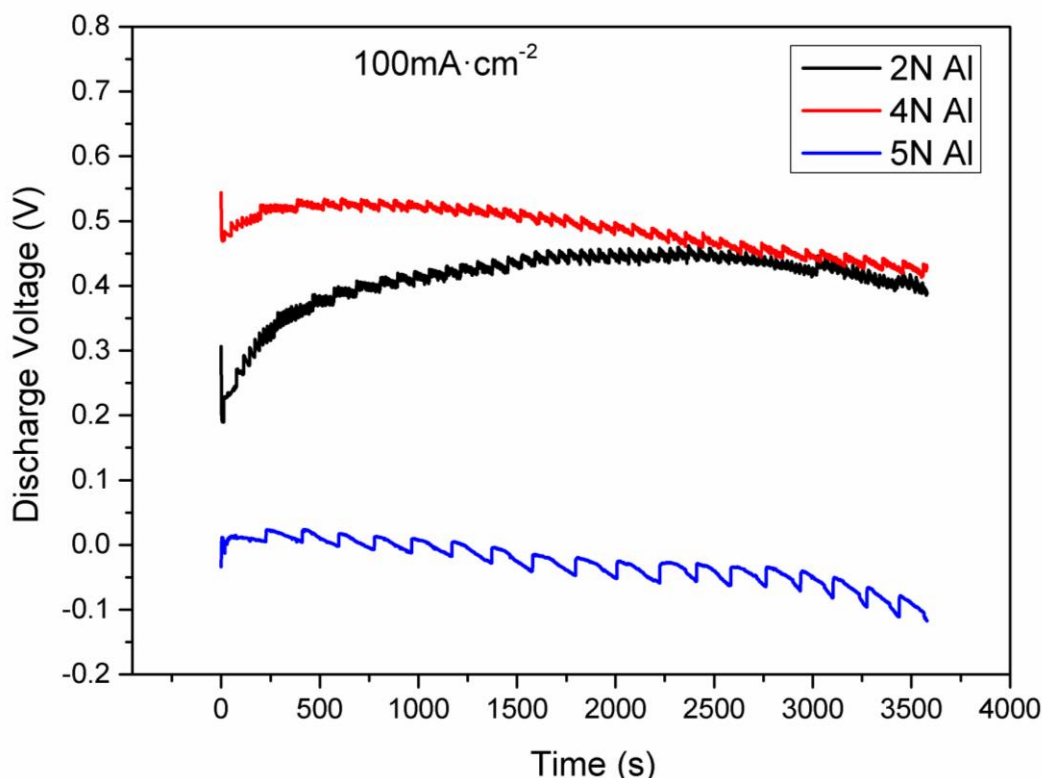
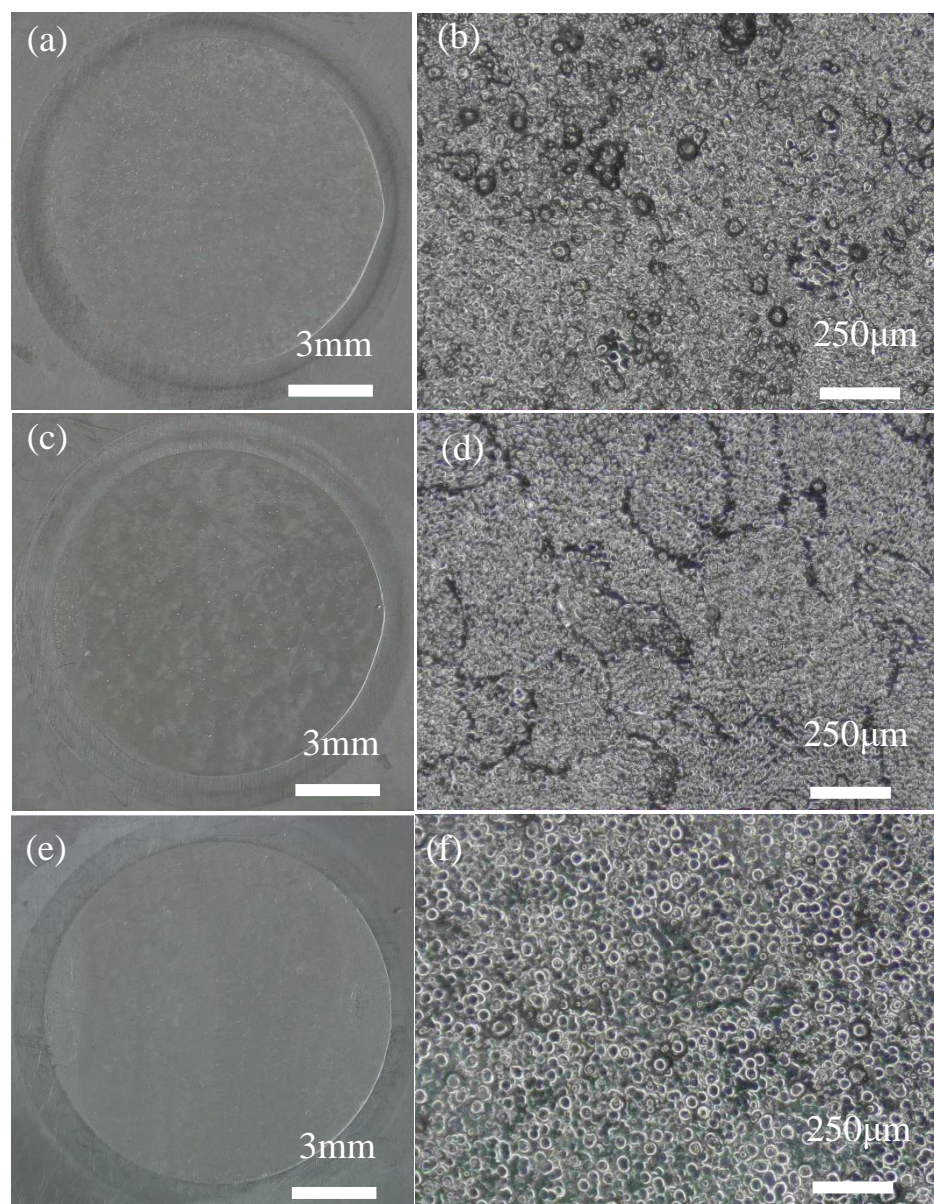


Figure 11. Cell voltage vs time curves of three grades purity Al at current density of $100 \text{ mA}\cdot\text{cm}^{-2}$ for the full-cell in 4 M NaOH solutions

Table 5. Batteries performance parameters for three grades of purity Al discharged at current density of 100 mA·cm

	Average Discharge Voltage(V)	Anode Utilization (η , %)	Capacity Density (mAh·g ⁻¹)	Energy Density (Wh·kg ⁻¹)
2N Al	0.41	33	982	452
4N Al	0.48	61	1810	833
5N Al	-	-	-	-

**Figure 12.** The morphologies of Al anode after discharge at current density of 100 mA·cm⁻² for the full-cell in 4 M NaOH solutions (a,b) 2N Al; (c,d) 4 N Al; (e,f) 5N Al

4. CONCLUSIONS

The discharge and corrosion behavior of Al anodes with different purity in alkaline solution were systematically studied. With the decrease of Al purity, the self-corrosion resistance of Al anode decreases whereas the electrochemical activity increases. The self-corrosion resistance is determined by Fe-bearing impurity particles. The electrochemical activity depends on both Fe-bearing impurity particles and the solid solubility of Fe impurity element in Al matrix. Fe dissolution into Al matrix increases the OCP and then decreases the operating voltage. Fe-bearing impurity particles act as an activator for the initial oxide film on Al anodes, resulting in a decrease of cathodic and anodic polarization. Based on the effect of Fe impurity element on the self-corrosion and electrochemical activity in three purity Al anodes, 4N Al exhibits high operating voltage and discharge efficiency, regardless of at low or high constant current density.

ACKNOWLEDGEMENTS

This work is financially supported by Anhui Provincial Natural Science Foundation (1808085ME123), the Projects of International Cooperation and Exchanges in Anhui Provincial Key Project of Research and Development Plan (1804b06020363), the Key University Science Research Project of Anhui Province (KJ2017A054), Priority Funding Scheme for Innovative Projects for Overseas Chinese Students in Anhui Province.

References

1. E.I. Shkolnikov, A.Z. Zhuk, M.S. Vlaskin, *Renewable Sustainable Energy Rev.*, 15 (2011) 4611.
2. A.V. Ilyukhina, B.V. Kleymentov, A.Z. Zhuk, *J. Power Sources*, 342 (2017) 741.
3. S.H. Yang, H. Knickle, *J. Power Sources*, 112 (2002) 162.
4. B.B. Chen, D.Y.C. Leung, *J. Electrochem. Energy Convers. Storage*, 13 (2016) 1.
5. H. Moghanni-Bavil-Olyaei, J. Arjomandi, M. Hosseini, *J. Alloys Compd.*, 695 (2017) 2637.
6. A.M.M.M. Adam, N. Borrás, E. Pérez, P.L. Cabot, *J. Power Sources*, 58 (1996) 197.
7. H. Moghanni-Bavil-Olyaei, J. Arjomandi, *RSC Adv.*, 6 (2016) 28055.
8. S. Zein EL Abedin, A.O. Saleh, *J. Appl. Electrochem.*, 34 (2004) 331.
9. I. Smoljko, S. Gudic, N. Kuzmanic, M. Kliskic, *J. Appl. Electrochem.*, 42 (2012) 969.
10. V. Volkov, S. Eliseeva, A. Pimenov, A. Shvarev, *Inter. J. Electrochem. Sci.*, 11 (2016) 8981.
11. T. Xu, Z.F. Hu, C. Yao, *Inter. J. Electrochem. Sci.*, 14 (2019) 2606.
12. L. Gnana Sahaya Rosilda, M. Ganesan, M. Anbu Kulandainathan, V. Kapali, *J. Power Sources*, 50 (1994) 321.
13. M. Paramasivam, G. Suresh, B. Muthuramalingam, S. Venkatakrishna Iyer, V. Kapali, *J. Appl. Electrochem.*, 21 (1991) 452.
14. V. Kapali, S. Venkitakrishna Iyer, N. Subramanyan, *Br. Corros. J.*, 4 (1969) 305.
15. X.Y. Wang, J.M. Wang, H.B. Shao, J.Q. Zhang, C.N. Cao, *J. Appl. Electrochem.*, 35 (2005) 213.
16. E. Grishina, D. Gelman, S. Belopukhov, D. Starosvetsky, A. Groysman, Y. Ein-Eli, *ChemSusChem.*, 9 (2016) 1.
17. J.J. Ma, W.H. Li, G.X. Wang, Y.Q. Li, F.Z. Ren, Y. Xiong, *J. Electrochem. Soc.*, 165 (2018) 266.
18. Y.F. Wang, H. Kwok, W.D. Pan, H.M. Zhang, D.Y.C. Leung, *J. Power Sources*, 414 (2019) 278.
19. B.J. Hopkins, Y.S. Horn, D.P. Hart, *Nature*, 362 (2018) 658.
20. Z. Zhang, C.C. Zuo, Z.H. Liu, Y. Yu, Y.X. Zuo, Y. Song, *J. Power Sources*, 251 (2014) 470.
21. M.A. Deyab, *Electrochim. Acta*, 244 (2017) 178.

22. L. Fan, H.M. Lu, *J. Power Sources*, 284 (2015) 409.
23. Y. J. Cho, I. J. Park, H.J. Lee, J.G. Kim, *J. Power Sources*, 277 (2015) 370.
24. M.L. Doche, F. Novel-Cattin, R. Durand, J.J. Rameau, *J. Power Sources*, 65 (1997) 197.
25. I. John Albert, M. Anbu Kulandainathan, M. Ganesan, V. Kapali, *J. Appl. Electrochem.*, 19 (1989) 547.
26. D.J. Hansen, F.E. Wetmore, *Can. J. Chem.*, 34 (1956) 659.
27. K. Mizuno, A. Nylund, I. Olefjord, *Corros. Sci.*, 43 (2001) 381.
28. S. Khireche, D. Boughrara, A. Kadri, L. Hamadou, N. Benbrahim, *Corros. Sci.*, 87 (2014) 504.
29. N. Birbilis, R.G. Discussion, *J. Electrochem. Soc.*, 152 (2005) B140.
30. C. Vargel, *Corrosion of Aluminium*, Elsevier, 2004.
31. P. L. Rossiter, *The Electrical Resistivity of Metals and Anodes*, Cambridge university press, 1987, p.9.
32. K. Liu, X. Cao, X.G. Chen, *Metall. Mater. Trans. A*, 42 (2011) 2004.
33. S.M. Gerchakov, L.R. Udey, F. Mansfeld, *Corrosion*, 37 (1981) 696.
34. C.M.A. Brett, *Corros. Sci.*, 33 (1992) 203.
35. M. Keddad, C. Kuntz, H. Takenouti, D. Schuster, D. Zuili, *Electrochim. Acta*, 42 (1997) 87.
36. S. Gudic, I. Smoljko, M. Kliskic, *Mater. Chem. Phys.*, 121 (2010) 561.
37. R.N. Mutlu, S. Ates, B. Yazici, *Inter. J. Hydrogen Energ.*, 42 (2017) 23315.
38. J.J. Ma, F.Z. Ren, G.X. Wang, Y. Xiong, Y.Q. Li, J.B. Wen, *Inter. J. Hydrogen Energ.*, 42 (2017) 11654.
39. M.C. Reboul, PH. Gimenez, J.J. Rameau, *Corrosion*, 40 (1984) 366.
40. M.L. Doche, J.J. Rameau, R. Durand, F. Novel-Cattin, *Corros. Sci.*, 41 (1999) 805.